EXTRAPOLATION FROM WIND TUNNEL TO FLIGHT: SHUTTLE ORBITER AERODYNAMICS

J.Muylaert, L.Walpot - ESA-ESTEC, The Netherlands
P.Rostand, M.Rapuc - Dassault Aviation, France
G.Brauckmann, J.Paulson, D.Trockmorton, K.Weilmuenster - NASA LaRC, USA

ABSTRACT

The paper reviews a combined numerical and experimental activity on the Shuttle Orbiter, first performed at NASA Langley within the Orbiter Experiment (OEX) and subsequently at ESA, as part of the AGARD FDP WG 18 activities. The study at Langley was undertaken to resolve the pitch up anomaly observed during the entry of the first flight of the Shuttle Orbiter. The present paper will focus on real gas effects on aerodynamics and not on heating. The facilities used at NASA Langley were the 15-in. Mach 6, the 20-in, Mach 6, the 31-in. Mach 10 and the 20-in. Mach 6 CF4 facility. The paper focuses on the high Mach, high altitude portion of the first entry of the Shuttle where the vehicle exhibited a nose-up pitching moment relative to pre-flight prediction of $(\Delta C_m) = 0.03$. In order to study the relative contribution of compressibility, viscous interaction and real gas effects on basic body pitching moment and flap efficiency, an experimental study was undertaken to examine the effects of Mach, Reynolds and ratio of specific heats at NASA. At high Mach, a decrease of gamma occurs in the shock layer due to high temperature effects. The primary effect of this lower specific heat ratio is a decrease of the pressure on the aft windward expansion surface of the Orbiter causing the nose-up pitching moment. Testing in the heavy gas, Mach 6 CF4 tunnel, gave a good simulation of high temperature effects.

The facilities used at ESA were the 1m Mach 10 at ONERA Modane, the 0.7 m hot shot F4 at ONERA Le Fauga and the 0.88 m piston driven shock tube HEG at DLR Goettingen. Encouraging good force measurements were obtained in the F4 facility on the Orbiter configuration. Testing of the same model in the perfect gas Mach 10 S4 Modane facility was performed so as to have "reference" conditions. When one compares the F4 and S4 test results, the data suggests that the Orbiter "pitch up" is due to real gas effects. In addition, pressure measurements, performed on the aft portion of the windward side of the Halis configuration in HEG and F4, confirm that the pitch up is mainly attributed to a reduction of pressure due to a local decrease in gamma.

1 Introduction

During the high Mach number, high altitude segment of the first entry of the Space Shuttle Orbiter, with laminar, continuum flow over the windward surface, the vehicle exhibited a nose-up pitching-moment increment (ΔC_m) relative to pre-flight prediction of approximately 0.03. This caused the body-flap to deflect twice the amount thought necessary to achieve trimmed flight. This so-called "pitch-up anomaly" has been investigated over the years with explanations ranging from compressibility, to viscous, to real-gas (high temperature) effects on basic-body pitching moment and/or body-flap effectiveness. Compressibility and viscous effects, while affecting basic aerodynamics, also govern the behavior of flow separation ahead of deflected control surfaces. Low values of Reynolds number, such as occur in flight at high altitudes, may cause the flap to lose effectiveness by submerging it in a thick boundary layer such that the flap does not encounter the inviscid flow. In addition, high viscous shear of the cross flow in the nose region has been postulated as the mechanism to induce nose-up pitching moments. High-temperature effects occur when the free stream gas crosses the strong bow shock of the vehicle in hypersonic flight. The main consequences relative to perfect gas as far as aerodynamics are concerned are an increase in the shock density ratio, hence decrease in shock detachment distance and altering of the inviscid flow field, and a lowering of the flow field specific heat ratio.

In order to clarify and substantiate the causes of the flight-to-preflight discrepancies, a systematic study was undertaken to examine the effects of Mach number, Reynolds number, and real gas effects on basic-body pitching moment and body-flap effectiveness.

At NASA, two approaches were used by Brauckmann, Paulson, and Weilmuenster (1995). First, conventional hypersonic wind tunnels, all with instrumentation upgrades and most with new nozzles

that provide better flow uniformity, were used to examine the effects of Mach number and Reynolds number on configuration aerodynamics and control effectiveness. Effects due to specific-heat ratio were examined in the 20-Inch Mach 6 CF_4 tunnel, where testing in a heavy gas simulates the higher normal shock density ratio and lower specific heat ratio characteristic of that experienced in flight. Second, a Navier-Stokes computer code utilizing finite-rate chemistry was used to predict the flow field over the entire orbiter windward geometry, including the deflected body-flap, for both wind tunnel and flight conditions ((Weilmuenster, Gnoffo, and Greere 1993)). Comparisons are made between the present experimental results, computational predictions, the preflight aerodynamic data book released in 1980 and aerodynamic coefficients derived from the Space Shuttle Orbiter flights specially that of STS-1. The results of this study are expected to help define the optimum approach for the design of the next generation space transportation system.

At ESA, the orbiter model was used for a study by Perrier, Rapuc, P.Rostand, Sagnier, Verant, Eitelberg, Bogstad, and Muylaert (1996) on hypersonic wind tunnel to flight extrapolation. The objective of the study presented here is to investigate the extent to which the use of high enthalpy facilities can contribute to the validation of such a ground to flight extrapolation, and more specifically to the validation of "real gas effects". Such high enthalpy facilities, where both forces and heat fluxes can be measured, have been developed recently in Europe, and preliminary encouraging results have been obtained on simple shapes such as Electre model, which is a blunt cone and a hyperboloid flare ((Muylaert, Walpot, and Durand 1993)). A methodology to validate the ground to flight extrapolation of re-entry aircraft aerodynamics is proposed and implemented in the case of the Orbiter, based on the utilization of European high enthalpy facilities, and theoretical rebuilding of the flow fields in these facilities and in flight . It is shown that uncertainties on the real gas effect on aerodynamic forces, and in particular on pitching moment, could be reduced through this procedure.

2 Experimental methods

2.1 NASA Facilities

Three models were used for this study. Two were scale models of the full Shuttle Orbiter configuration, with scales of .004 and .0075. Body-flap deflections tested were 0.0, 12.5, and 16.3 deg for the smaller model and 0.0, 16.0, and 20.0 deg for the larger model. The third model was a .0075 scale modified Orbiter geometry, referred to as Halis, which accurately represented the windward surface, including the body-flap, but used elliptical cross-sections to create the upper surface. All models were numerically machined from stainless steel. A verification check of the aerolines was performed prior to testing, and both larger models represented the shuttle windward surface aerolines within +/− .003 in. Five blow-down hypersonic wind tunnels were used in this study . They were the 15-Inch Mach 6 Hi-Temperature Air Tunnel, 20-Inch Mach 6 Tunnel, 31-Inch Mach 10 Tunnel, 22-Inch Mach 20 Helium Tunnel, and the 20-Inch Mach 6 CF_4 Tunnel at NASA Langley. (See table 2)

All data are presented about a moment reference center of 65 % of reference body length.

2.2 European Facilities

In Europe, 2 Orbiter models and 3 hypersonic facilities were used for the present study as seen from table 2. The 3 facilities are the ONERA S4 , The ONERA F4 and the DLR HEG.

The ONERA S4 facility is a Mach=10 perfect gas blow down tunnel. It is considered as the European reference perfect gas Mach 10 facility. It was decided to run it at its lowest Re number corresponding to a reservoir pressure of 25 Bar so as to avoid boundary layer transition in separated shear layers in front of deflected flaps.

The ONERA F4 hot shot , is a high enthalpy facility which enables force and moment measurements. The F4 facility covers enthalpy levels corresponding to the dissociation of oxygen. Typical reservoir conditions are 500 bar with 250 reduced enthalpy (Hi/RTo, R= 288.2 J/kg/K for air, To = 273.15 K), i.e 19.7 MJ/kg. The lowest total conditions are about 200 Bar and Hi/RTo = 30. (i.e. 23.61 Mj/kg) High pressure and low enthalpy levels can also be obtained such as Pi = 750 Bar and Hi/RTo = 30, (i.e. 23.61 Mj/kg). The test gas used is synthetic air or N2.

The DLR HEG free piston driven shock tunnel allows both oxygen and nitrogen dissociation and presents higher enthalpy levels and Reynolds numbers than F4. Typical reservoir pressure conditions are 1000 Bar combined with a reservoir enthalpy which can vary between 10 MJ/kg up to 25 MJ/kg.

3 Computational Methods

The NASA results presented were obtained with the LAURA code (Langley Aerothermodynamic Upwind Relaxation Algorithm) ((Gnoffo 1990)) was used in this study to solve the thin-layer Navier-Stokes equations. The inviscid first-order flux is constructed us-

ing Roe's flux-difference-splitting ((Roe 1983)) and Harten's entropy fix with second order corrections based on Yee's symmetric total variation diminishing scheme ((Harten 1983)). A seven species (N, O, N_2, O_2, NO, NO^+, and e^-) chemical reaction model is used for the non-equilibrium computations. The usual no-slip boundary conditions for viscous flow is applied at the wall while freestream conditions are set at points on the outer boundary of the computational domain. The exit plane is set such that the inviscid outer flow is supersonic. The computations presented account for a variable wall temperature. These values are based on the radiation equilibrium temperature at the wall, and were determined from computed heating rates. A catalytic wall boundary condition was used based on Scott's recombination rates for nitrogen and Zoby's rates for oxygen ((Scott 1981; Zoby, Gupta, and Simmons 1985)). A multiblock solution strategy is applied in two stages. The first stage may be regarded as a space marching solution, like the Parabolized Navier-Stokes (PNS) methods, except three-dimensional data blocks are employed rather than two-dimensional data planes. The second stage is a conventional, global relaxation which uses the first stage solution as an initial condition. The computational results presented herein are discussed further, and with more detail about the code and solution procedure in papers by (Weilmuenster, Gnoffo, and Greere 1993).

In Europe, Dassault Aviation used an Euler and boundary layer approach rather than a Navier Stokes approach, in order to perform a large number of simulations at a reasonable cost.

The Euler code used is the EUGENI code of Dassault Aviation, which solves the compressible fluid equations discretized on an unstructured mesh, for a perfect gas or a reacting mixture, either in equilibrium or in chemical or thermochemical non-equilibrium. Implicit time integration to the steady state is used; convergence requires 100 to 500 iterations, depending on cases and accuracy requirements. The solver is based on a Galerkin finite volume method, in which inviscid fluxes are upwinded using a generalized version of Osher's Riemann solver. Second order accuracy is achieved using the MUSCL method, extended to unstructured meshes.

The finite rate dissociation of air is modeled with 5 species (O2, O, N2, N and NO) and 34 reactions. The rates are taken from Park's model. The finite rate thermal relaxation is modeled with two vibrational temperatures and one translational and rotational temperature.

The boundary layer code used is the COUL code of Dassault Aviation, which is a package containing different boundary layer solvers, ranging in complexity from integral method based codes to finite difference defect correction based ones, and able to take into account finite rate chemistry. The solver used here is the finite difference defect correction one, with finite rate chemistry and second order matching with the inviscid flow field (for velocity, temperature and concentrations).

4 NASA Results and Discussion

4.1 Ideal Gas Results at Mach 6 and 10 in Air

For the low-to-mid hypersonic Mach numbers the flight-to-preflight aerodynamic discrepancy is small. Post-flight analysis of heating data indicate that the orbiter windward surface boundary layer is everywhere turbulent. Experimental results at Mach 6 are presented showing the effect of Reynolds number on C_N and C_m for the baseline (zero control surface deflections) in Figures 1 and 2, respectively. The experimental data show only a slight effect of Reynolds number. C_N is decreased, and C_m is slightly nose-down with increasing Reynolds number; however, it should be noted that most of this is within the accuracy of the data, especially for the lower Reynolds numbers (and hence dynamic pressure). Results for a body-flap deflection of 16.0 deg are shown in Figures 3 and 4. C_N is approximately the same for all Reynolds numbers, indicating an increase relative to the baseline configuration. Pitching moment shows a marked nose-down increment with increasing Reynolds number, indicating a more effective body-flap as Reynolds number increases. The cause of these effects can be traced to changes in the location of boundary layer separation and re-attachment in front of and on the body flap. Surface-streamline patterns (oil flows) on the windward surface in the vicinity of the body-flap are shown in Figures 5 to 8. The model is at an angle of attack of 40 deg with a body-flap deflection of 16.0 deg. As Reynolds number increases, the separation region decreases. While the forward separation line moves rearward a small amount, the main effect is the forward motion of the re-attachment line on the flap itself. The separation is not as well defined at a length Reynolds number of $1.6x10^6$; the oil appearing somewhat smeared or "runny". Several repeat runs were made which verified this pattern. It is postulated that the flow is, or is near, transitional; at the next Reynolds number tested, $Re_\infty = 3.2x10^6$, the flow overcomes the pressure gradient due to the deflected flap and remains attached on the whole lower surface, and the oil flow appears clear and sharp again. Similar aerodynamic and oil-flow results were observed at Mach 10. The data and oil flow photographs can be found in Brauckmann, Paulson, and Weilmuenster (1996). At $M_\infty = 10$, no limiting case

of flap effectiveness was obtained, as at $M_\infty = 6$, presumably due to insufficient Reynolds number variation to achieve transitional flow. Comparisons of the current $M_\infty = 6$ and $M_\infty = 10$ results to the preflight prediction (ADDB) and to STS-1 mission flight-derived data points are made in Figures 9 and 10. The highest Reynolds number experimental data are used. All data are interpolated at flight values of α, referenced to a center-of-gravity location of 0.65L, and the flight derived data points have been adjusted to zero-control surface deflection using the ADDB effectiveness values. The agreement of the current values of C_N with the data book is very good. Both the current data and the preflight prediction overestimate the the flight C_N by a slight amount. The agreement in pitching moment is not as good, especially at Mach 10. Values from the ADDB are in-between the current data and flight. The discrepancy between the current wind tunnel data and flight represents a movement in center of pressure location of 7.7 inches, or 0.6 % of the body length. It is probable that non-ideal gas effects are present. Also, recall that the flight data were corrected using ADDB control surface effectiveness values. Body-flap effectiveness, ΔC_m, at $M_\infty = 6$ and 10 is compared to the preflight prediction in Figure 11. Reynolds number plays a small role on basic-body pitching moment at these Mach numbers, primarily affecting body-flap effectiveness. As just shown, predicted body-flap effectiveness is bounded; i.e the current data at Mach=6 and 10 are in general less than ADDB. While not duplicating the preflight data book, the current tests are in line with the results. Conventional hypersonic wind tunnels (non-impulse) are therefore able to accurately describe the aerodynamics of this class of entry vehicles at these low to mid hypersonic Mach numbers. Proper determination of flight control surface effectiveness requires proper simulation of the state of the boundary layer (i.e. laminar, transitional, or turbulent).

5 Computational Predictions

Computational fluid dynamics (CFD) were used to examine differences between ideal gas and real-gas flow fields. Ideal gas flow fields can be duplicated in the wind tunnel, whereas in this study real-gas effects were only simulated. Solutions for the modified orbiter geometry corresponding to wind tunnel and flight conditions were obtained at angles of attack of 35, 40, 45 deg for body-flap deflections of 0, 5, 10, 15, and 20 deg. The data were interpolated for body-flap deflections of 16.0 and 16.3 deg, to compare with data presented from the wind tunnel tests. A more complete discussion of these results can be found in a paper by Weilmuenster ((Weilmuenster, Gnoffo, and Greere 1993)). The predictions were in good qualitative agreement, although the code over-predicted C_N by about 2.5 %. Differences in C_m amounted to 1 % error in center of pressure location. In order to examine the differences in the flow field that occur in flight, computations were carried out using finite-rate chemistry on the modified orbiter geometry at flight conditions. As shown in Figure 12, the occurrence of high temperatures associated with this flight condition dissociates the flow within the shock layer such that the ratio of specific heats, γ, defined here as h/e, is reduced from 1.4 in the freestream, to 1.3 immediately behind the shock to about 1.14 near the body. In the nose region, γ is reduced to about 1.12. The major effect of this change in γ is a lowering of the surface pressure on the last 20 % of the vehicle. A plot of computed center-line surface pressure for wind tunnel and flight conditions is given in Figure 13. Included are results from Weilmuenster, Gnoffo, and Greere (1993) a solution at a Mach number of 24 using an ideal gas value for γ of 1.4. There is a small difference due to Mach number alone, but the largest difference is due to the lower γ. The lower γ results in the expansion on the aft end occurring to a greater degree, lowering the pressure over a large area of the vehicle. It should be noted that the Orbiter geometry has a large influence on the magnitude of the real-gas effects. The Orbiter has an expansion that starts at approximately 0.8L, which coincides with the largest planform area, and thus the greater expansion of the flow, relative to ideal gas flow, lowers the pressure over a large area. The impact of this reduced pressure on the aerodynamic coefficients is shown in Figures 9 and 17. The lower pressure on the aft end causes a reduction in normal force and a nose up pitching-moment increment. The computed increment in C_N between tunnel and flight conditions is .062 and .048 for $\delta_{BF} = 0.0$ deg and 16.3 deg, respectively. This agrees well with the delta found in flight, $\Delta C_N = .059$ (preflight ADDB-to-flight, STS-1). The increment in C_m for $\delta_{BF} = 0.0$ deg is 0.040, which is larger than the increment found between flight and pre-flight prediction. For the 16.3 deg flap case however, the delta is 0.028, which is very close to that found between the preflight ADDB and flight. The difference in the two increments can be traced to greater flap effectiveness at flight conditions. There are two reasons for the greater calculated flap effectiveness. The predicted separation region in front of and on the flap is smaller in flight than in the wind tunnel, for the same length Reynolds number. Calculated streamline patterns in the region of the body-flap at both tunnel and flight conditions for two flap deflections are shown in Figures 14 and 15. The much smaller separation region for flight conditions is evident. In addition, as discussed by Weilmuenster the pressure rise on the flap was higher in flight than in the wind tunnel, but this was due to a combination of Mach

and γ effects. In fact, the lower γ tends to reduce the pressure rise, but the higher Mach number in the shock layer in flight overcomes this. A solution at $M_\infty = 24$ (flight) but with $\gamma = 1.4$ (ideal gas) was not obtained on the deflected flap configuration, thus a separation of these effects cannot be made. An analysis of control-surface effectiveness was performed after the first few flights of the Shuttle Orbiter. Both an elevon and a body-flap pulse maneuver were analyzed in terms of center-of-pressure location for predicted and flight performance. While the results were biased from the perfect correlation line, the conclusion was reached that flap effectiveness, as presented in the preflight ADDB, was predicted correctly. More analysis of this discrepancy is needed.

6 High Mach Number Simulation

Two facilities at Langley were used to examine the high Mach number flight regime, the 22-Inch Mach 20 Helium Tunnel and the 20-Inch Mach 6 CF_4 Tunnel. The 22-Inch Helium Tunnel uses purified helium which behaves as an ideal gas with a γ of 1.667. There are a number of advantages to testing with helium, the primary one being that very high values of Re_L may be generated at high Mach numbers without having to heat the gas to prevent liquefaction. For this study, the facility provided a close match of flight Mach and Reynolds numbers. However, the flow field γ remained at γ =1.667. The results from the helium tunnel tests showed a significant nose-down pitching moment compared to flight, which can be explained by γ being higher rather than lower than ideal air. In addition, body flap effectiveness was reduced. Thus, testing in helium is inappropriate for the simulation of real-gas effects. The CF_4 tunnel uses a heavy gas which has a γ lower than ideal air to simulate this aspect of real-gas flows such as occurs in flight. The value of γ in the CF_4 tunnel, around 1.15 in the shock layer, is close to that determined to occur in flight. A comparison of aerodynamic coefficients obtained in air and CF_4 at identical values of Reynolds number and Mach number is given in Figures 18 and 19. As can be seen, testing in a heavy gas decreases the normal force coefficient and causes a nose-up pitch increment, when compared with results in air. At 40 degree of incidence, the decrease in C_N is 0.046 for $\delta_{BF} = 0.0$ deg and .077 for $\delta_{BF} = 16.3$ deg. This decrement is approximately the same as the flight decrement and that determined by the CFD analysis . The change in C_m is .029 for $\delta_{BF} = 0.0$ deg and .027 for $\delta_{BF} = 16.3$ deg. This increment is the same as the flight-to-preflight increment. The increment is the same for both the undeflected and deflected body-flap configurations as seen experimentally in figure 18. For this configuration then, with an expansion region on the windward surface, the real-gas effects are closely approximated by testing in a heavy gas such as CF_4

7 ESA results and discussion

7.1 Methodology

The process of ground to flight extrapolation is the following :

1. Definition of reference conditions in perfect gas hypersonic facilities.
2. Reduction of aerodynamic uncertainties for these reference conditions through comparisons with results from different sources, both experimental and computational and analysis of all possible sources of errors (shape inaccuracies in wind tunnel or CFD model, inadequate flow modeling, biased instrumentation..).
3. Transposition to flight : utilization of the same prediction method for the reference and flight conditions.
4. Analysis of the differences in terms of flow physics between wind tunnel and flight and derivation of the uncertainties in the process of transposition.
5. Establishment of the preflight uncertainties in the predictions for flight conditions, as the sum of the uncertainties for the reference conditions and those due to the transposition process.

The purpose here is to investigate to what extend the use of high enthalpy facilities can contribute to the validation of the real gas effects in this process of ground to flight extrapolation. The F4 and HEG facilities represent two intermediate steps between the S4 perfect gas conditions and the flight conditions, on which CFD results can be cross-checked in the process of extrapolation to flight.

The real gas effects which can be expected in each of these impulse facilities are presented in figures 21 and 22, in the form of dissociation level, equivalent γ and Damkholer number versus enthalpy, for flight and wind tunnel conditions, behind a normal shock wave (representing the stagnation point) and behind a 40 degree shock wave (representing the aft part of forebody) , assuming thermochemical equilibrium. The conditions are those following a typical Orbiter trajectory. Figure 20 shows the preflight to flight discrepancy for STS 5. The flight data is for the Orbiter flying at a trim condition, hence a zero pitching moment. The predicted results are those based

on the preflight aerodynamic database and for the flight aerodynamic control settings. It can be seen from figure 20 that the γ effect appears for relatively moderate enthalpies, corresponding to flight Mach numbers of about 10. Indeed the analysis of flight results shows that, when the Mach numbers increases, the pitch-up appears at Mach=10 and stabilizes at Mach=16 . The two high enthalpy facilities are in the range of enthalpies representative of this *gamma* effect, and so should be quite representative of the pitch-up effect expected. This *gamma* effect, since it is a function of the derivative of the equation of state ($C^2 = \partial P/\partial \rho$), appears as soon as deviation from perfect gas occurs, i.e. as soon as vibrational energy appears, which for oxygen is around 2000 K.

Equilibrium dissociation levels are also significant in the ground facilities for oxygen; however for nitrogen only HEG can give a limited dissociation, and only in the stagnation area. It must be recalled however that actual dissociation levels in the ground facilities could be much smaller due to the very low Damkholer numbers. This means that finite rate effects can be expected to be significantly different between ground and flight conditions.

The base line flight point chosen is the following:

STS-2, time: 75620s

Mach number: 24.3

Altitude: 72.3 km

Angle of attack: 39.40 degrees

Elevon deflection: 1.70 degrees

Body flap deflection: 14.90 degrees

Computations and wind tunnel tests are performed for the following configuration:

Angle of attack: 40 degrees

Elevon deflection: 0 degrees

Body flap deflection: 0 and 15 degrees

Corrections for the slightly different angle of attack and deflections are introduced in the comparisons.

For the purpose of analysis, the real gas effect is subdivided in three elements:

- the equilibrium chemistry effect, defined as the difference between results with equilibrium chemistry assumption and those with perfect gas,γ=1.4 assumption.
- the effect of finite rate chemistry, defined as the difference between results with finite rate chemistry and those with equilibrium chemistry.
- the effect of finite rate thermal relaxation defined as the difference between results with finite rate chemistry and thermal relaxation and those with finite rate chemistry only.

For comparison between flight and ground facility results, the effect of Mach number must be defined also, as the difference between results obtained at flight and ground facility Mach numbers, using the perfect gas, γ=1.4 assumption.

Computations have been performed with the corresponding modeling for the four conditions investigated here (S4 "blow down", F4 "hot shot", HEG "shock tube" and flight). The conditions are summarized in the table 2.

7.2 High Enthalpy Simulation

This chapter will cover both results from the numerical computations carried out on the Orbiter as well results from high enthalpy testing. The shape of both the Orbiter and Halis are described by CAD files provided by NASA. The geometry of the Orbiter includes accurate representations of all items except windshield and elevon gaps. The aircraft surface is represented with an unstructured triangular mesh made of 7000 nodes in the case of the Orbiter and 6000 in the case of Halis. The volume mesh is built by an advancing front method from the skin mesh, and is made of tetrahedras. Its unstructured nature facilitates the clustering of the mesh points in the shock layer. The volume mesh of the Orbiter contains 130000 nodes and that of Halis 113 000 nodes. In order to compute the flow field around models in high enthalpy facilities, it is necessary to first rebuild the flow in the facilities' nozzle, since complex phenomena are expected in these nozzles, and significant uncertainties exist in their prediction. The flow field is rebuilt using CFD, in which unknown parameters, such as transition point of the boundary layer, are tuned in order to match measurements made at the nozzle wall and exit. The computed nozzle exit plane is then used as inflow conditions for the computations of the flow around the model.

The computed pitching moment of the US Orbiter is represented in figures 23 to 26, and compared to experimental data. It is given for the flight center of gravity, angle of attack and elevon deflection, as defined in previous paragraph, and for 0 degrees and 15 body-flap deflection. Ground facility and flight conditions are referenced in these figures by total enthalpy, which is the primary parameter controlling the chemistry effects; however other parameters, such as pressure or Mach number also play a role, so that the data presented should not be interpreted as a direct pitch(enthalpy) function, but rather as a pitch(real gas effect) one, the scale for the real gas effect being qualitative. In figure 23 the pitching moment for the Orbiter with no flap deflection is presented for S4, F4 and flight conditions, from computations with four different gas models (perfect gas, equilibrium chemistry, finite rate chem-

istry, finite rate chemistry and thermal relaxation), and from experiment. In figure 24 the same data is presented collapsed to its S4 value, which is the reference point. The S4 computations were subtracted from the computations corresponding to higher enthalpy; the S4 experimental data were subtracted from those of F4. The difference between the S4 experiments and computations can be reduced by approximately half if special attention is given to grid refinements and base correction. In addition the force and moment measurements were performed on the "Orbiter model" whereas the computations on the HALIS configuration which contains a simplification of the leeward side. Consequently figure 24 illustrates best the transposition to flight of the pitching moment for the Orbiter with no flap deflection. It is seen that for flight conditions the major part of the real gas effect can be accounted for using equilibrium chemistry, finite rate chemistry effect being much smaller, and finite rate thermal relaxation playing no role. The effect shown for the F4 enthalpy conditions is essentially the same as for the flight conditions. At the F4 condition, the experimental results falls roughly midway between the calculated results assuming equilibrium and nonequilibrium. However, the equilibrium solution produces the big change with respect to the perfect gas solution as it did for the flight condition. Then the nonequilibrium calculation produces a significant but more modest correction to the equilibrium results. It is seen also that the computational and experimental results agree best on the S4 to F4 transposition if the flow is assumed to be in equilibrium.

In figures 24 to 26 the comparison of results for different conditions, and transposition to flight, are presented for the case with 15 degrees body flap deflection and for the body-flap efficiency, using the same method as for the 0 degree case. In figure 26, again, the same data as from figure 24 are shown but collapsed to its S4 value.

It must be recalled however that the computations have been performed with an Euler code, and that although a viscous correction, derived from previous studies ((Perrier, Rapuc, P.Rostand, Sagnier, Verant, Eitelberg, Bogstad, and Muylaert 1996)), has been introduced, the objective here is not to predict the control surface efficiency itself but the effect of air dissociation on this efficiency.

It is seen on figures 25 and 26 that the pitching moment for HEG conditions is lower than for F4 conditions, i.e. that the "real gas effect" on pitch in HEG is lower than in F4; this is somewhat surprising but could be explained by the evolution of the "equivalent γ" with enthalpy, figure 22, which is not monotonic. More numerical analysis is needed to understand why the calculated pitching moment for HEG conditions are lower than those obtained in F4 conditions. Figure 26 shows the body flap efficiency defined as the ratio of the pitching moment difference between bodyflap 15 degree and 0 degrees with the corresponding difference as obtained in the reference S4 conditions. It can be seen that the flap efficiency is much higher in flight than in F4, suggesting that not just Reynolds but also γ and local Mach number play a role. In addition, the analysis need to be completed with a discussion of wall temperature effects on boundary layer development and resulting pitching moment. Indeed we should not forget that in high enthalpy short duration facilities like F4 and HEG, wall temperature are ambient temperature whereas in flight radiative equilibrium wall temperatures are obtained.

Pressure coefficient distribution along the windward centerline are presented in figure 28 for S4, F4 and HEG conditions and for the non deflected body-flap configuration. These distributions confirm the pitch up described in the previous chapter since one can notice between S4 and F4 a small pressure coefficient increase at the nose and larger decrease at the rear. Less difference are visible between S4 and HEG, indicating that the pitch up would be smaller.

The pressure distributions obtained for the four conditions investigated are presented in figures 29 to 32, and compared to experimental data in figures 33 to 35. The real gas effect is very local, and occurs mainly in the expansion and secondary compression areas, i.e. in front of the body flap and at the leading edges / corners of the fuselage and wing, so that only the pitching moment is significantly affected by the real gas effect (lift and drag changes are small).

7.3 Ground to flight transposition

7.3.1 Reference "cold" uncertainties

The rebuilding of the cold reference point is an important part of the ground to flight extrapolation process, as presented in the introduction. In order to reduce the uncertainties to a minimum, it is necessary, in the framework of a design study, to perform mesh refinement studies, and to compare the results coming from a large number of sources. Also all differences and inaccuracies in the shape must be tracked and accounted for.

Such a study, which is quite lengthy, has been performed for Hermes ((Perrier, Rapuc, P.Rostand, Sagnier, Verant, Eitelberg, Bogstad, and Muylaert 1996)); here our main effort is on the transposition process, and the uncertainties on the predictions for the reference point, although reasonable, could be further reduced: the discrepancy between CFD and experimental results in terms of pitching moment is equivalent to a 3 degree deflection of the body-flap;

on the body-flap efficiency it is 6 %; The wind tunnel results are in good agreement with the computations, in terms of pitching moment, so that the remaining discrepancies between CFD and experiment are due to insufficient griding or more probably to small inaccuracies in the CFD shape.

7.3.2 Influence of real gas effects

For the flight point chosen the real gas effects can be decomposed in the following way (0 body flap deflection):

- Effect of Mach number :+ 0.0045
- Total real gas effect: 0.0332
  - Effect of equilibrium chemistry : + 0.038
  - Effect of finite rate chemistry : - 0.0055
  - Effect of finite rate thermal relaxation :+ 0.0007

On the control surface efficiency, the real gas effect can be decomposed similarly (excluding coupling between chemistry and viscous interactions):

- Effect of Mach number : - 1%
- Total real gas effect: + 22%
  - Effect of equilibrium chemistry : + 26%
  - Effect of finite rate chemistry : - 4%

7.3.3 Assessment of uncertainties

The effect of equilibrium chemistry on pitching moment is of the same order of magnitude in F4 and flight conditions; also better agreement is obtained between CFD and experiment in F4 if equilibrium flow is assumed. The effect of finite rate chemistry and thermal relaxation is not validated at this stage. However in flight these elements only contribute to 15 % of the real gas effects; consequently the uncertainties they induce are quite small. In the present example , the dispersion on real gas effect on pitching moment between experimental results and CFD results obtained with equilibrium chemistry is 8 % for the case with no body flap deflection and 13 % for the case with 15 degree body flap deflection. (This latter number includes dispersion due to approximate representation of viscous interactions) If the uncertainty of the effect of finite rate is taken arbitrarily to be 50 % , then the total uncertainty on the real gas effect can be estimated as follows in table 1. The total uncertainty is the sum of an 8 % (13 % for the case with 15 degree deflection) dispersion for equilibrium chemistry applied on the 115 % of the total real gas effect and a 50 % dispersion

Nature	Contribution to real gas effect,%	Intrinsic uncertainty,%	Contribution to global uncertainty
Equilibrium chemistry	115%	8%	9.2%
Finite rate	−15%	50%	7.5%
Total	100%		16.7%

Table 1: Total uncertainty on the real gas effect

applied on 15 % of the total real gas effect, and so is globally 17 % (22 % for the 15 degree body flap case).

The figures above for dispersion can be reduced through the use of Navier Stokes equations due to improved representation of viscous interaction effects.

The mentioned 17 % uncertainty on the orbiter pitching moment is equivalent to a 1.9 degree body flap deflection, which is coherent with a discrepancy between flight data and prediction equivalent to a 1.3 degree deflection.

8 SYNTHESIS AND CONCLUSION.

A study was undertaken at the NASA Langley Research Center to resolve the cause of the "pitch-up anomaly" observed during entry of the first flight of the Shuttle Orbiter. At high Mach flight conditions a reduction in specific heat ratio occurs due to high temperature effects. The primary effect of this lower specific heat ratio within the flow field of the Orbiter is lower pressures on the aft windward expansion surface of the Orbiter, relative to those deduced from hypersonic wind tunnel tests with ideal or near ideal gas test flows, and thus a corresponding nose-up pitching moment. Computationally, good agreement with the flight aerodynamic coefficients was obtained with the flap deflected to approximately 16 deg. Testing in a heavy gas in the 20-Inch Mach 6 CF_4 Tunnel gave a good simulation of high temperature effects as the aerodynamic increments and flap effectiveness were in good agreement with flight results. The overall agreement between flight, computational solutions at flight conditions (laminar boundary layer, continuum flow regime), and measurements made in the CF4 tunnel was quite good. This study has demonstrated a preferred approach to test high fidelity models in conventional facilities to provide base-line data for design; combined with the use of the heavy gas facility for the simulation of the high temperature effects. Complementary CFD to be used for substantiating these results as well as to provide information at flight conditions.

AT ESA, through Dassault Aviation, a procedure to validate ground to flight extrapolation of re-entry spacecraft aerodynamics has been proposed and im-

plemented in the case of the Orbiter, using European high enthalpy facilities. Encouraging results have been obtained for force coefficients, leading to a possible method to significantly reduce the uncertainties in the transposition to flight and in particular the uncertainties associated with real gas effects.

REFERENCES

Brauckmann, G., J. Paulson, and K. Weilmuenster (1995, September). Experimental and computational analysis of the space shuttle orbiter hypersonic pitch-up anomaly. *AIAA Journal of Spacecraft and Rockets 32*(5), 758–764.

Brauckmann, G., J. Paulson, and K. Weilmuenster (1996, January). Experimental and computational analysis of the space shuttle orbiter hypersonic 'pitch-up anomaly'. In *AIAA Conference*, Reno, USA. AIAA paper 94-0632.

Gnoffo, P. (1990). An upwind point implicit relaxation algorithm for viscous compressible perfect-gas flows. Technical Report TP 2953, NASA.

Harten, A. (1983). High resolution schemes for hyperbolic conservation laws. *Journal of Computational Physics 49*, 357–393.

Muylaert, J., L. Walpot, and G. Durand (1993, 6-9 July). Computational analysis on generic forms in european hypersonic facilities: standard model Electre and hyperboloid flare. In *19th International Symposium on Shock Waves (ISSW19)*, Marseille.

Perrier, P., M. Rapuc, P.Rostand, P. Sagnier, J. Verant, G. Eitelberg, M. Bogstad, and J. Muylaert (1996, June). Ground to flight extrapolation of reentry aircraft aerodynamics: an experimental and computational approach. In *AIAA 14th Applied Aerodynamics Conference*, New Orleans, USA. AIAA paper 96-2434.

Roe, P. (1983). Approximate Riemann solvers, parameters vectors and difference schemes. In *Journal of Computational Physics*, Volume 43, pp. 357–372.

Scott, C. (1981). Catalytic recombination of oxygen and nitrogen in high temperatures surface insulation. *Aerothermodynamics and Planetary Entry. 77*, 192–212.

Weilmuenster, K., A. Gnoffo, and A. Greere (1993, 6-9 July). Navier-stokes simulations of the shuttle orbiter aerodynamic characteristics with emphasis on pitch trim and body flap. In *AIAA 28th Thermophysics Conference*, Orlando, FL.

Zoby, E., R. Gupta, and A. Simmons (1985). Temperature dependant reaction rate expressions for oxygen recombination. *Thermal Design of Aeroassisted Orbital Transfer Vehicles 96*, 445–465.

TUNNEL	Mach no.	Scale	$Re_{\infty,L}, 10^6$	γ_∞	Pt (Psia)	Tt(^0F)
15-in. Mach 6	6.0	0.004	0.2	1.4	45	780
			1.7		240	470
20-in. Mach 6	6.0	0.0075	0.4	1.4	30	400
			0.8		60	425
			1.6		125	450
			3.2		250	475
			6.1		475	475
31-in. Mach 10	10.0	0.0075	0.4	1.4	350	1350
			0.9		720	1350
			1.8		1450	1350
20-in. Mach 6 CF_4	6.0	0.004	0.2	1.22	1600	800

Table 2: NASA LaRC facilities for Orbiter testing

FACILITIES	ONERA S4 MA	ONERA F4	DLR HEG	FLIGHT
TYPE	BLOW DOWN	HOT SHOT	SHOCK TUBE	
MODEL SCALE	1/90	1/90	1/90	1/1
MACH NUMBER	10	8	10	24
Hi/RT	14	160	280	330
Res.PRESSURE(bar)	25	280	450	
ALTITUDE(km)				72
REYNOLDS(10^{-5})	6.	0.3	1.2	10
PL/V 10^6	3.6	0.044	0.12	0.28
MEASUREMENTS	FORCES	FORCES		
	PRESSURE	PRESSURE	PRESSURE	
	HEAT FLUX	HEAT FLUX	HEAT FLUX	

Table 3: ESA facilities for Orbiter testing

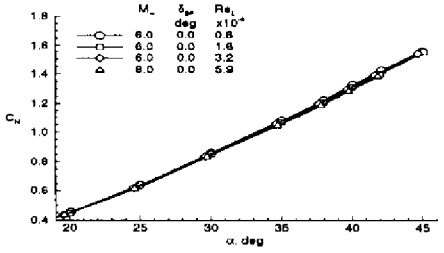

Figure 1: Effect of Re-number on Shuttle Orbiter on C_N for body flap 0 degrees

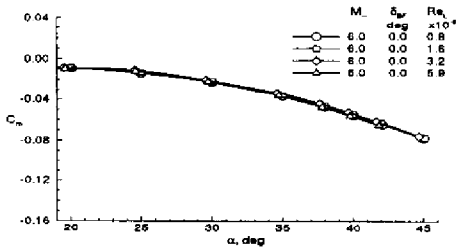

Figure 2: Effect of Re-number on Shuttle Orbiter on C_m for body flap 0 degrees

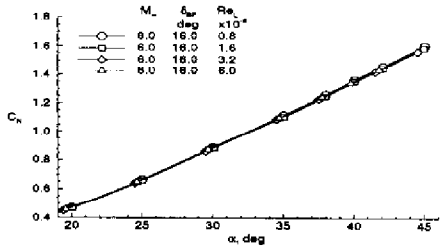

Figure 3: Effect of Re-number on Shuttle Orbiter on C_N for body flap 16 degrees

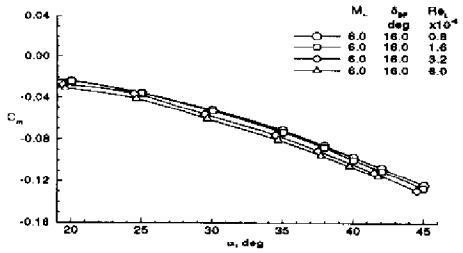

Figure 4: Effect of Re-number on Shuttle Orbiter on C_m for body flap 16 degrees

Figure 5: Oil flow for $Re_L = 0.4x10^6$

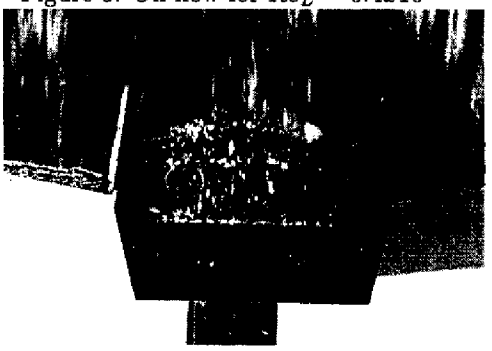

Figure 6: Oil flow for $Re_L = 0.8x10^6$

Figure 7: Oil flow for $Re_L = 1.6x10^6$

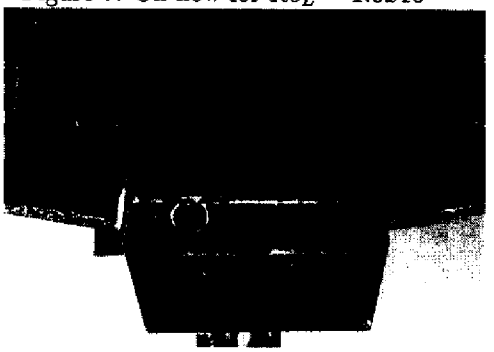

Figure 8: Oil flow for $Re_L = 3.2x10^6$

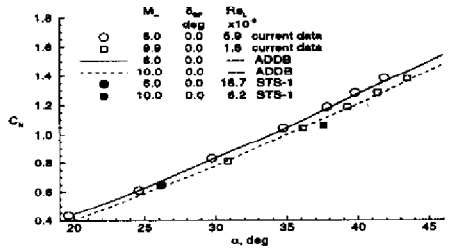

Figure 9: Comparison of C_N for current experimental data with ADDB and flight

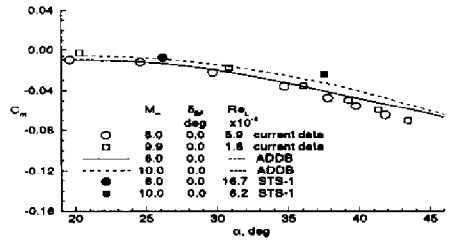

Figure 10: Comparison of C_m for current experimental data with ADDB and flight

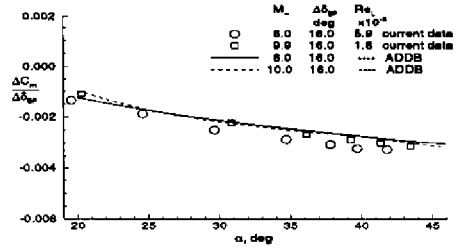

Figure 11: Comparison of flap efficiency for current experimental data with ADDB and flight

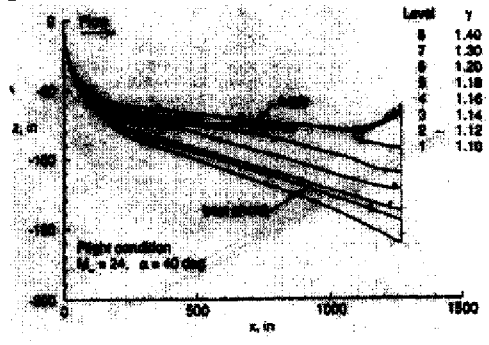

Figure 12: Computed variation of γ in windward flow field of modified Orbiter

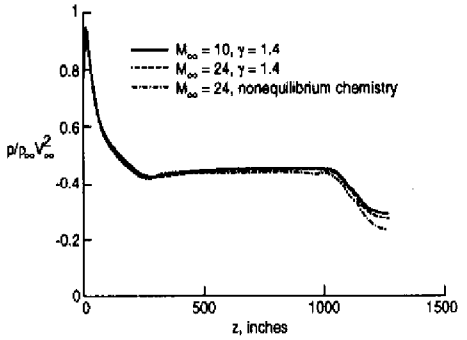

Figure 13: Computed centerline surface pressure for modified Orbiter, α =40°

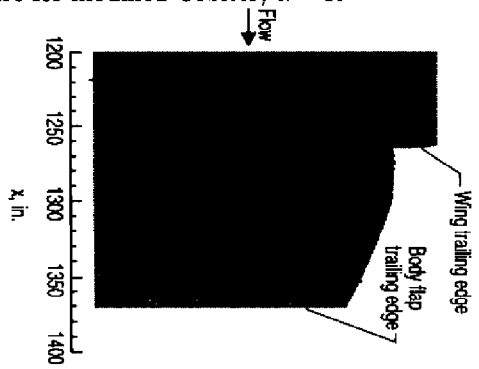

Figure 14: Calculated surface streamline patterns in vicinity of body flap at wind tunnel conditions

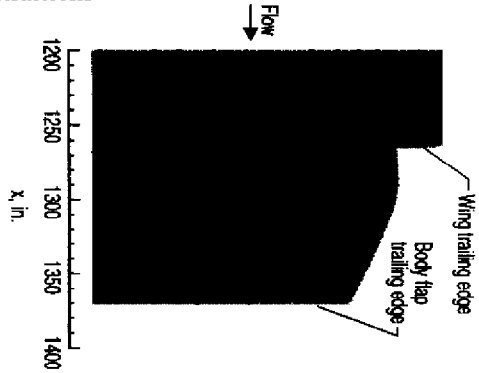

Figure 15: Calculated surface streamline patterns in vicinity of body flap at flight conditions

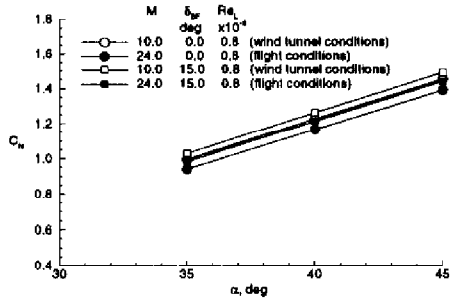

Figure 16: Comparison of computed modified Orbiter C_N at wind tunnel and flight conditions

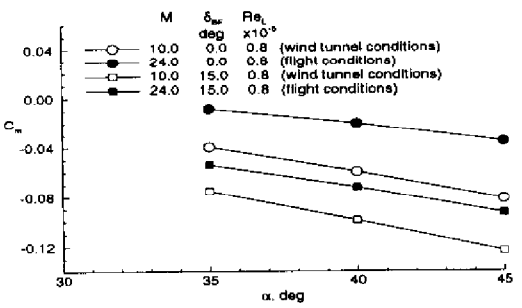

Figure 17: Comparison of computed modified Orbiter C_m at wind tunnel and flight conditions

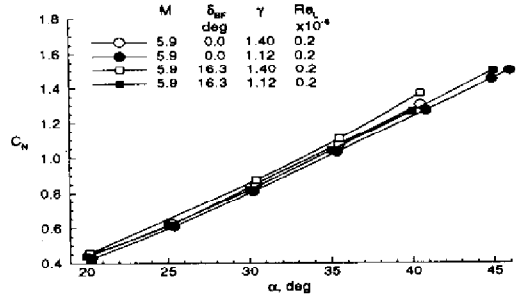

Figure 18: Comparison of Shuttle Orbiter aerodynamics in air and CF_4

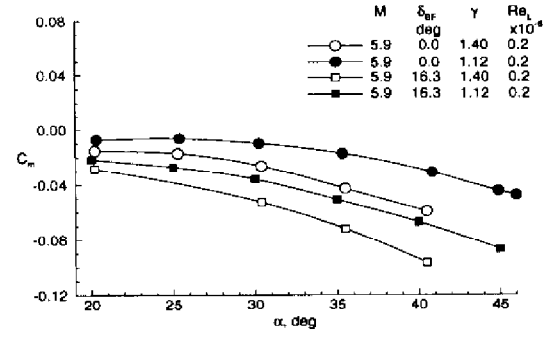

Figure 19: Comparison of Shuttle Orbiter aerodynamics in air and CF_4: wind tunnel data

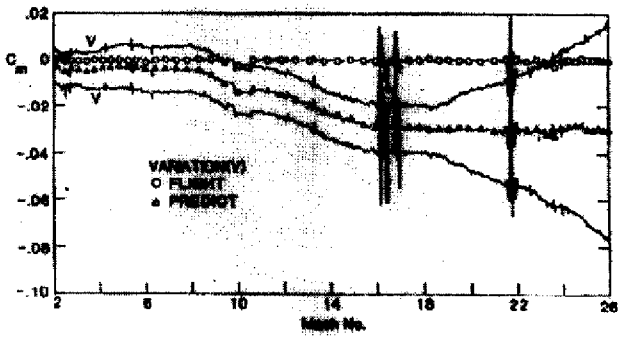

Figure 20: Pre-flight to flight discrepancy for STS-5

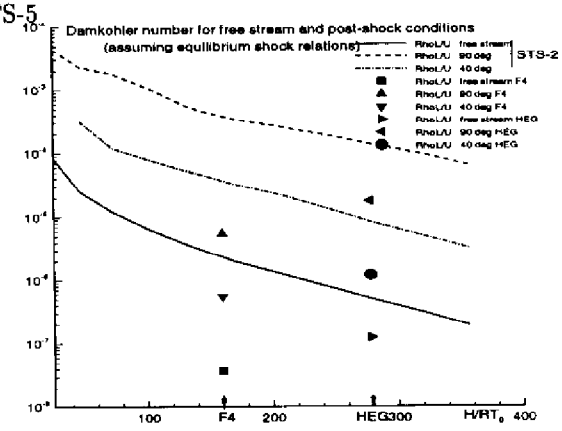

Figure 21: Damkohler number in terms of $\rho L/V$ for free stream and post-shock conditions assuming assuming equilibrium flow, plotted versus reduced enthalpy following STS2 trajectory or for F4, HEG wind tunnel conditions.

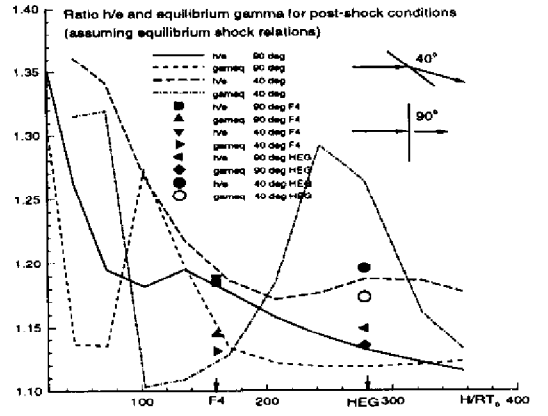

Figure 22: Equivalent γ's behind a 40 or 90 degree shock wave assuming equilibrium flow, plotted versus reduced enthalpy following STS2 trajectory or for F4, HEG wind tunnel conditions.

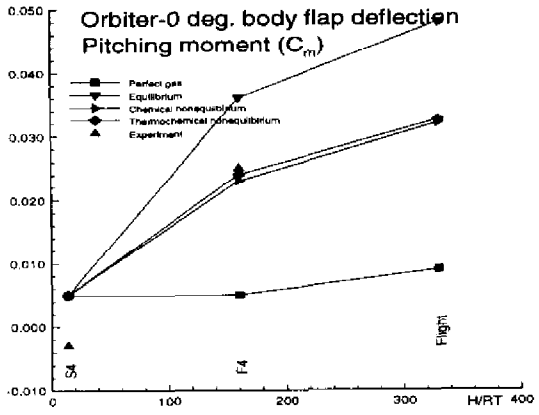

Figure 23: Pitching moment of the Shuttle Orbiter with 0 degrees body flap deflection; Cm pitching moment versus reduced enthalpy.

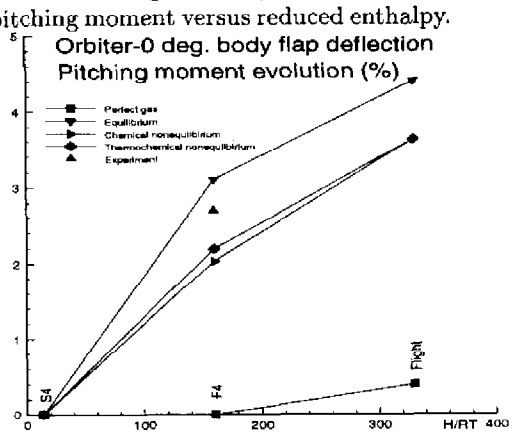

Figure 24: Pitching moment evolution of the Shuttle Orbiter with 0 degrees body flap deflection; % pitching moment referenced to S4 results.

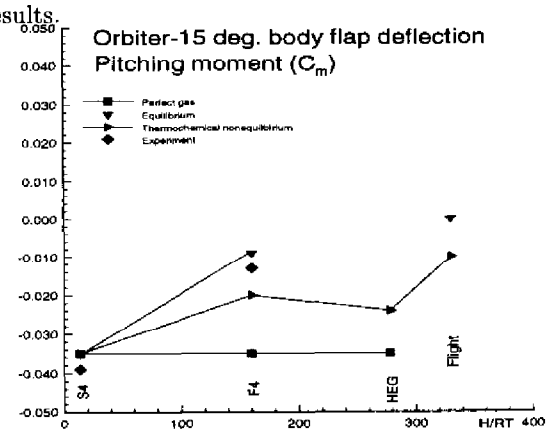

Figure 25: Pitching moment of the Shuttle Orbiter with 15 degrees body flap deflection; Cm pitching moment versus reduced enthalpy.

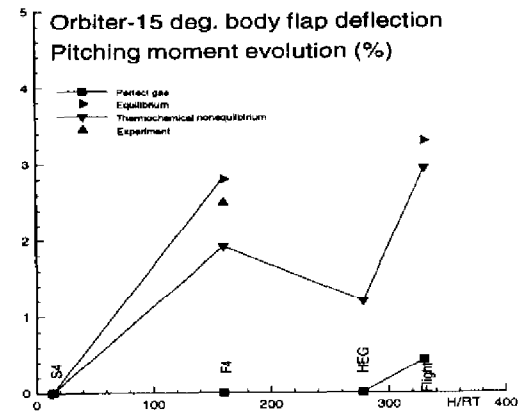

Figure 26: Pitching moment evolution of the Shuttle Orbiter with 15 degrees body flap deflection; % pitching moment referenced to S4 results.

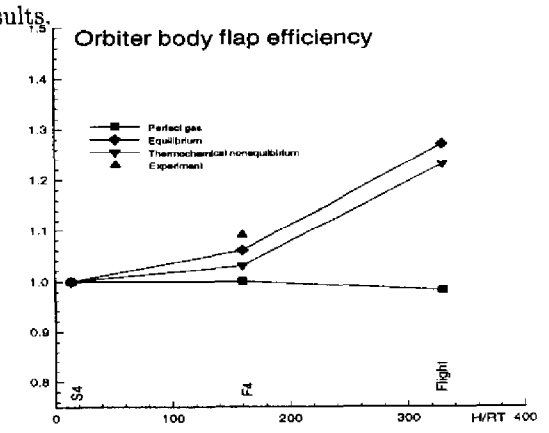

Figure 27: Flap efficiency of the Shuttle Orbiter.

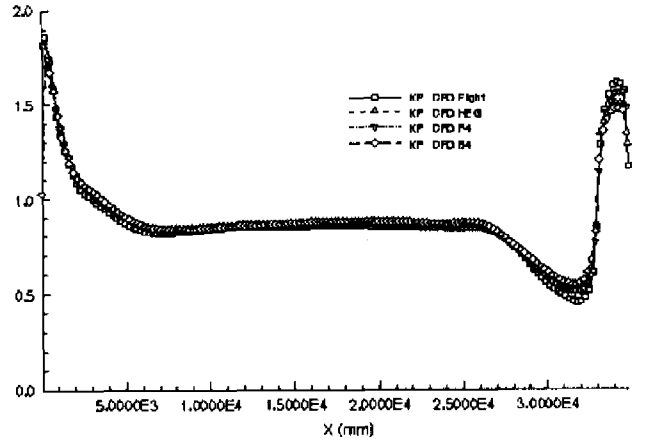

Figure 28: Centerline pressure coefficient distribution on HALIS.

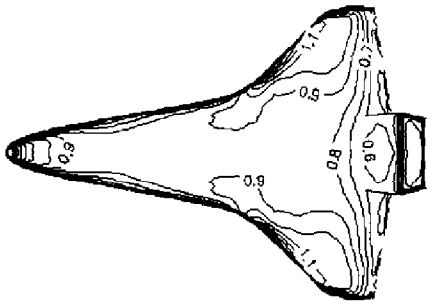

Figure 29: Pressure coefficient distribution for S4 conditions.

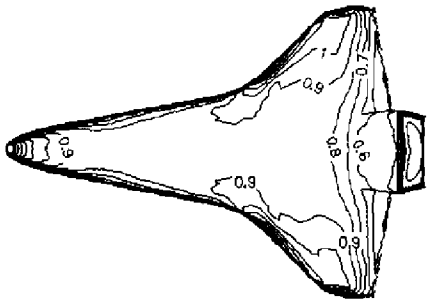

Figure 30: Pressure coefficient distribution for F4 conditions.

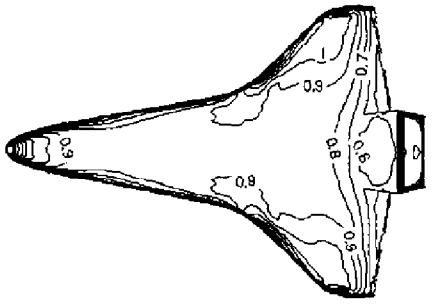

Figure 31: Pressure coefficient distribution for HEG conditions.

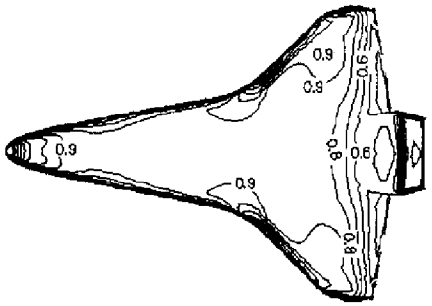

Figure 32: Pressure coefficient distribution for flight conditions.

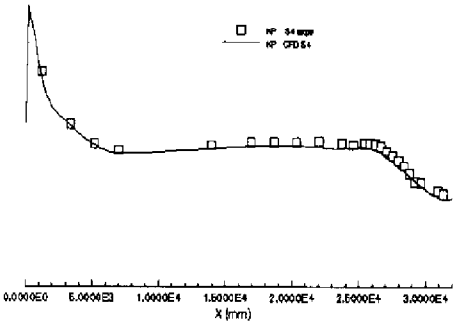

Figure 33: Pressure distribution on the symmetry line of HALIS, compared to experimental data, at S4 conditions.

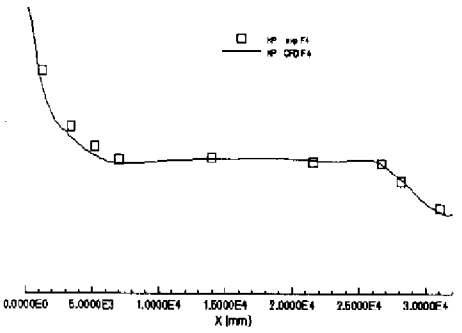

Figure 34: Pressure distribution on the symmetry line of HALIS, compared to experimental data, at F4 conditions.

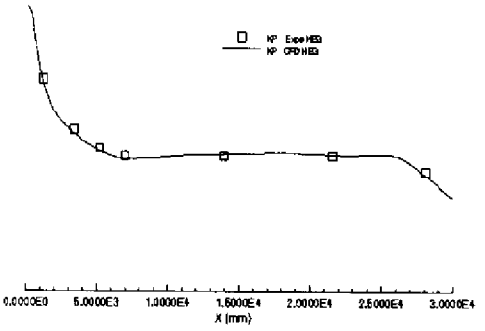

Figure 35: Pressure distribution on the symmetry line of HALIS, compared to experimental data, at HEG conditions.